

Soft X-ray emission lines of Fe XV in solar flare observations and the Chandra spectrum of Capella

F. P. Keenan¹, J. J. Drake², S. Chung², N. S. Brickhouse², K. M. Aggarwal¹, A. Z. Msezane³, R. S. I. Ryans¹ and D. S. Bloomfield¹

F.Keenan@qub.ac.uk

ABSTRACT

Recent calculations of atomic data for Fe XV have been used to generate theoretical line ratios involving $n = 3-4$ transitions in the soft X-ray spectral region ($\sim 52-83$ Å), for a wide range of electron temperatures and densities applicable to solar and stellar coronal plasmas. A comparison of these with solar flare observations from a rocket-borne spectrograph (XSST) reveals generally good agreement between theory and experiment. In particular, the 82.76 Å emission line in the XSST spectrum is identified, for the first time to our knowledge in an astrophysical source, as the $3s3d\ ^3D_3-3s4p\ ^3P_2$ transition of Fe XV. Previous suggested identifications of the 53.11, 63.97 and 69.65 Å features as the $3s^2\ ^1S-3s4p\ ^3P_1$, $3p^2\ ^1D-3s4f\ ^1F$ and $3s3p\ ^1P-3s4s\ ^1S$ lines of Fe XV, respectively, are confirmed. However the former is blended (at the $\sim 50\%$ level) with the S IX $2s^22p^4\ ^3P_1-2p^33s\ ^3P_2$ transition. Most of the Fe XV transitions which are blended have had the species responsible clearly identified, although there remain a few instances where this has not been possible. The line ratio calculations are also compared with a co-added spectrum of Capella obtained with the *Chandra* satellite, which is probably the highest signal-to-noise observation achieved for a stellar source in the $\sim 25-175$ Å soft X-ray region. Good agreement is found between theory and experiment, indicating that the Fe XV lines are reliably detected in *Chandra* spectra, and hence may be employed as diagnostics to determine the temperature and/or density of the emitting plasma. However the line blending in the *Chandra* data is such that individual emission lines are difficult to measure accurately, and

¹Department of Physics & Astronomy, Queen's University Belfast, Belfast, BT7 1NN, Northern Ireland, U.K.

²Smithsonian Astrophysical Observatory (SAO), MS 3, 60 Garden Street, Cambridge, MA 02138

³Center for Theoretical Studies of Physical Systems, Clark Atlanta University, Atlanta, GA 30304

fluxes may only be reliably determined via detailed profile fitting of the observations. The co-added Capella spectrum is made available to hopefully encourage further exploration of the soft X-ray region in astronomical sources.

Subject headings: Atomic data – Sun: flares – Stars: late-type – X-ray: spectra

1. Introduction

Emission lines arising from $n = 3$ – 3 transitions in Fe XV are widely detected in solar extreme ultraviolet (EUV) spectra covering the ~ 200 – 400 Å wavelength interval (Dere 1978; Thomas & Neupert 1994). The $3s^2\ ^1S$ – $3s3p\ ^1P$ resonance line at 284 Å is one of the most intense emission features in the solar EUV spectrum, and has also been widely observed in stellar coronal sources by the *Extreme Ultraviolet Explorer* (EUVE) satellite (Laming & Drake 1999). Bely & Blaha (1968) first noted the potential of EUV lines of Fe XV as diagnostics for the emitting plasma, and since then many authors have calculated emission line intensities for this ion and compared these with solar observations (see, for example, Kastner & Bhatia 2001 and references therein).

However Fe XV also shows a rich emission line spectrum in the soft X-ray region, ~ 50 – 80 Å, arising from $n = 3$ – 4 transitions. By contrast to the EUV lines, there has been little work on the soft X-ray transitions in the astrophysical literature, probably as a result of the limited availability of high quality solar spectra for this wavelength region. There were several rocket-borne flights in the 1960’s which covered the soft X-ray region, but these detected few or no Fe XV transitions (see, for example, Austin et al. 1966; Widing & Sandlin 1968; Behring, Cohen, & Feldman 1972; Malinovsky & Heroux 1973). The most detailed measurements of the $n = 3$ – 4 lines in Fe XV to date were made by the XSST spectrograph during a rocket flight in 1982 (Acton et al. 1985). However, even these observations have only been subject to a brief analysis by Bhatia, Mason, & Blancard (1997), as part of their work to produce a large atomic dataset for this ion. Finally, Campbell & Brickhouse (2001) presented preliminary results from an investigation of Fe XV and Fe XVI lines in *Chandra* X-ray spectra of the late-type coronally-active stars Capella (G1 III + G8 III) and Procyon (F5 IV).

In this paper we use the most recent atomic physics calculations for Fe XV to generate soft X-ray line ratios for a wide range of electron temperatures and densities applicable to coronal plasmas. We compare these in detail with the XSST observations of Acton et al. (1985), to assess the usefulness of the Fe XV transitions as plasma diagnostics. However, in addition we analyse a *Chandra* spectrum of Capella constructed from multiple observations.

This co-added X-ray spectrum has one of the highest signal-to-noise ratios ever achieved for an astrophysical coronal plasma in the $\sim 25\text{--}175$ Å soft X-ray region, hence allowing us to perform an investigation of the Fe XV $n = 3\text{--}4$ lines in an astronomical source other than the Sun.

The Capella spectrum is also made freely available, to encourage further research on the soft X-ray spectral region. For example, in conjunction with the published XSST solar line list, the Capella data should be useful for reliably identifying new emission features. In addition, there are potentially many useful diagnostic lines in the soft X-ray wavelength range, especially for solar flare-type plasmas (see, for example, Brown et al. 1986; Feldman et al. 1992), and hence further exploration and assessment of these is warranted.

2. Theoretical Line Ratios

The model ion for Fe XV consisted of the energetically lowest 53 fine-structure levels belonging to the $3s^2$, $3s3p$, $3p^2$, $3s3d$, $3p3d$, $3d^2$, $3s4s$, $3s4p$, $3s4d$, $3p4s$ and $3s4f$ configurations. Energies of these levels were obtained from Churilov et al. (1985), Churilov, Levashov, & Wyart (1989), Litzen & Redfors (1987), Sugar & Corliss (1985) and Aggarwal, Keenan, & Msezane (2003).

Electron impact excitation rates for transitions among all the levels discussed above were taken from Aggarwal et al. (2003). For Einstein A-coefficients, the calculations of Deb, Aggarwal, & Msezane (1999) were employed for allowed and intercombination lines. Radiative rates for forbidden transitions have also been taken from the work of Deb et al., although the data were not included in the published paper for conciseness. However we note that they are available from one of the authors (K.Aggarwal@qub.ac.uk) on request. Our A-value results for the forbidden transitions are, in general, very similar to those calculated by others, such as Bhatia et al. (1997). Proton impact excitation is only important for transitions among the $3s3p$ 3P levels of Fe XV, and in the present analysis we have employed the calculations of Landman & Brown (1979).

Using the atomic data discussed above in conjunction with a recently updated version of the statistical equilibrium code of Dufton (1977), relative Fe XV level populations and hence emission line strengths were calculated for a wide range of electron temperatures (T_e) and densities (N_e). Details of the procedures involved and approximations made may be found in Dufton, and Dufton et al. (1978).

In Figures 1–7 we plot the theoretical emission line intensity ratios R_1 through R_{11} , which are defined in Table 1. These ratios are shown as a function of T_e and/or N_e for a

range of temperatures ($T_e = 10^6$ – $10^{6.9}$ K) over which Fe XV has a fractional abundance in ionization equilibrium of $N(\text{Fe XV})/(\text{Fe}) > 10^{-3}$ (Mazzotta et al. 1998), and for values of N_e ($= 10^8$ – 10^{13} cm^{-3}) appropriate to solar and stellar coronal plasmas. In some instances, the ratios are predicted to be insensitive to electron density over the N_e interval considered (for example, R_1), in which case values are only plotted as a function of electron temperature at a single density. Others, such as R_2 , are weakly dependent on density, and hence are shown for a limited range of N_e values. However those ratios which vary significantly with T_e and N_e , such as R_4 , are plotted over the full range of plasma parameters. We note that the R_{12} ratio is not shown in the figures, as it has the same temperature and density dependence as R_5 , owing to common upper levels, but with

$$R_{12} = 2.95 \times R_5.$$

Given errors in the adopted atomic data of typically $\pm 10\%$ (see the references above), we would expect the theoretical ratios to be accurate to better than $\pm 20\%$.

The ratios in Figures 1–7 are given relative to the 59.40 Å transition, as this feature is the cleanest and most reliably detected Fe XV emission line in the soft X-ray spectral region. This has been checked by a search of line lists, and also by generating synthetic spectra with the latest version (4.2) of the CHIANTI database (Dere et al. 1997; Young et al. 2003), which confirm that no blending species is present which has a line intensity greater than 2% that of the Fe XV 59.40 Å feature. However we note that theoretical ratios involving any line pair are available electronically from one of the authors (FPK¹) on request.

An inspection of Figures 1–7 reveals that several of the ratios are sensitive to variations in the electron temperature and/or density. For example, R_7 varies by a factor of about 2.0 between $T_e = 10^6$ and $10^{6.9}$ K, while being insensitive to the adopted electron density. Similarly, R_{11} changes by a factor of 3.4 over the (relatively narrow) density interval of $N_e = 10^9$ – 10^{11} cm^{-3} at $T_e = 10^{6.3}$ K. Hence the ratios should, in principle, provide useful T_e – and/or N_e –diagnostics for the Fe XV emitting region of a plasma.

We note that the present theoretical line ratios are generally not excessively different from other recent calculations. For example, at $T_e = 10^{6.3}$ K and $N_e = 10^8$ cm^{-3} , we calculate $R_1 = 0.58$ compared to $R_1 = 0.68$ from CHIANTI and $R_1 = 0.38$ from Bhatia et al. (1997). Similarly, at these plasma parameters, we find $R_7 = 3.6$ compared to $R_7 = 3.5$ (CHIANTI) and $R_7 = 3.3$ (Bhatia et al.). However a notable exception is the R_2 ratio, for which we estimate $R_2 = 0.17$ at $T_e = 10^{6.3}$ K and $N_e = 10^8$ cm^{-3} , and Bhatia et al. calculate $R_2 = 0.11$. By contrast, CHIANTI indicates that $R_2 = 0.019$, a factor of 6–9 lower than the

¹F.Keenan@qub.ac.uk

other results. This discrepancy arises due to the adopted A-value for the $3s^2\ ^1S-3s4p\ ^3P_1$ transition. In our calculations, we use $A = 8.1 \times 10^{10}\ \text{s}^{-1}$ from Deb et al. (1999), and Bhatia et al. employ their own value of $A = 8.4 \times 10^{10}\ \text{s}^{-1}$. However the CHIANTI database uses $A = 1.5 \times 10^{10}\ \text{s}^{-1}$ from Griffin et al. (1999), which is significantly smaller than the other two calculations. Furthermore, Deb et al. undertook two independent calculations of radiative rates for Fe XV, using the CIV3 atomic structure code of Hibbert (1975) and the GRASP code of Dyllal et al. (1989). Their A-values for the $3s^2\ ^1S-3s4p\ ^3P_1$ transition from the two codes differ by only 11%, and as a consequence they assess that their calculations should be accurate to better than 20%. Given this, and the excellent agreement with the result of Bhatia et al., who also performed an independent calculation with the SUPERSTRUCTURE code of Eissner et al. (1972), we therefore believe that the Griffin et al. A-value is in error and should be re-evaluated.

3. Observational Data

We compare our Fe XV line ratio calculations with two datasets, namely that for a solar flare obtained with a rocket-borne spectrograph, and a composite spectrum for Capella observed with the *Chandra* satellite. These datasets are discussed separately below.

3.1. Solar flare observations

The solar spectrum analysed in the present paper is that of an M-class flare, recorded on Kodak 101–07 emulsion by an X-ray spectrograph (XSST) during a rocket flight on 1982 July 13. These observations spanned the wavelength range 11–97 Å, at a spectral resolution of 0.02 Å, and covered a solid angle of approximately 625 arcsec², centered on or near the brightest source of X-rays. The XSST made two exposures, one of 54 s beginning at 16:33:50 UT and the other of 145 s commencing at 16:35:35 UT. Unfortunately, a failure of the mechanism to move the film more than one mm between the two exposures resulted in their being nearly superimposed on the same plate. However, a careful analysis allowed the two spectra to be separated, so that analysis of the data could be performed, and the observations presented here are for the 145 s exposure. Further details of the XSST instrument may be found in Brown et al. (1979) and Bruner et al. (1980), while the observations are discussed in Acton et al. (1985).

It would clearly have been preferable to model the XSST observations in detail using profile fitting methods, as for the *Chandra* data (see § 3.2). This was unfortunately not

possible as the original XSST spectra are no longer available, following the retirement of several key staff involved in the mission. Consequently, only the published line list and intensities for XSST are now accessible. We have searched for Fe XV emission lines in the XSST spectrum, using the identifications of Acton et al. (1985) and also the NIST database² and other line lists, such as the Atomic Line List of Peter van Hoof³. In Table 1 we list the Fe XV transitions found in the spectrum, along with their measured wavelengths.

The intensity of the 59.40 Å line of Fe XV measured by Acton et al. (1985) in the XSST spectrum is given in Table 2; observed intensities of the other Fe XV transitions may be inferred from this using the line ratios given in the table (see § 2). Acton et al. (1985) note that a strong second-order spectrum falling between 25–50 Å is evident in the XSST observations, and that the effects of scattered light and double exposure made the reduction of the data difficult. However although difficult, Acton et al. did succeed in producing a well-calibrated spectrum and hence reliable measurements of emission line intensities. Evidence for this comes from, for example, our previous analysis of Ni XVIII emission lines in the XSST spectrum (Keenan et al. 1999). We found that, for 6 out of 7 line ratios involving Ni XVIII transitions in the 41–53 Å wavelength region, agreement between theory and observation is excellent, with differences that average only 11%. For the sole Ni XVIII line ratio which shows a large discrepancy between theory and observation, this is explained by a known blend with a Fe XIX transition. The Fe XV lines in the XSST spectrum should in fact be more reliably measured than those for Ni XVIII, as the former lie outside the 25–50 Å range affected by the second-order spectrum. Brown et al. (1986) and Keenan et al. note that the relative intensities of lines in the XSST spectrum similar in strength to the Fe XV transitions discussed here should be accurate to about $\pm 20\%$, and hence line ratios to $\pm 30\%$. The observed Fe XV line ratios in Table 2 have therefore been assigned a uniform $\pm 30\%$ uncertainty.

3.2. Capella Spectrum

3.2.1. Observations and Reduction

Capella is the mainstay target for calibrating and monitoring the *Chandra* transmission grating spectrometer dispersion relation. As such, it is currently observed approximately every 12 months using the LETG+HRC-S combination. The Capella observations anal-

²<http://physics.nist.gov/PhysRefData/>

³<http://star.pst.qub.ac.uk/~pvh/>

ysed here were obtained by the *Chandra* Low Energy Transmission Grating Spectrograph (LETGS), employing the High Resolution Camera spectroscopic detector (HRC-S) in its standard configuration, yielding spectra with a resolution of approximately 0.06 Å. (See Weisskopf et al. 2003 for a recent overview of the *Chandra* instrumentation and its in-flight performance). We have taken advantage of the multiple observations of Capella accrued to date to construct a composite spectrum with the highest signal-to-noise ratio possible. The different observations utilised, together with their dates of acquisition and exposure times, are listed in Table 3. Observations from 2002 were obtained at significantly different off-axis angles, and were not included in this analysis.

Data were uniformly processed and spectra extracted using the *Chandra* Interactive Analysis of Observations (CIAO) software Version 3.1. Photon event lists were also filtered in detector pulse height in order to remove particle-induced background events⁴. The final extracted co-added spectrum is shown in Figure 8, and we note that this is freely available from one of the authors (JJD⁵) electronically on request. In Figure 9 we plot the 50–75 Å portion of the spectrum, as this contains all of the Fe XV soft X-ray lines identified in Capella. Unfortunately, the spectrum is too noisy at longer wavelengths for other (weak) Fe XV features to be detected.

3.2.2. Analysis

The Capella spectrum was analysed using the PINTofALE⁶ IDL⁷ software suite (Kashyap & Drake 2000). Line fluxes were measured by fitting “modified Lorentzian”, or Moffat, functions of the form $F(\lambda) = a/(1 + \frac{\lambda-\lambda_0}{\Gamma})^\beta$, where a is the amplitude and Γ a characteristic line width. For a value of $\beta = 2.4$, it has been found that $F(\lambda)$ reproduces the line response function of the LETG+HRC-S instrument to the photometric accuracy of lines with a few thousand counts or less (Drake 2004). Uncertainties were estimated using a Monte Carlo sampling of the free parameters in the line fits.

Free parameters are, in general, the line width, position and amplitude, although for some of the fitting of poorer quality spectral features we constrained the line width to the value 0.065 Å found for nearby clean lines. Continua were estimated locally by eye for each

⁴See <http://cxc.harvard.edu/cal/Letg/Hrc.bg/>

⁵jdrake@cfa.harvard.edu

⁶Freely available from <http://hea-www.harvard.edu/PINTofALE/>

⁷Interactive Data Language, Research Systems Inc.

fit. Line positions were allowed to vary from their reference positions by $\leq 0.05 \text{ \AA}$, this being dictated by the imaging characteristics of the HRC-S detector. As discussed by Chung et al. (2004), the HRC-S exhibits small-scale imaging non-linearities that vary over the detector, and which can displace a spectral line from its true position by up to 0.05 \AA . While this effect can be calibrated to some extent using bright, well-known spectral lines, the wavelength range of interest to this Fe XV study is devoid of such transitions, and the characteristics of the imaging non-linearities have not been well defined in the relevant regions of the detector. For lines closely spaced in wavelength, the relative separations of the lines were kept fixed to their reference values, while the position of the group was allowed to vary. In the case of the group of lines in the $69.4\text{--}70.2 \text{ \AA}$ range (Figure 10), the wavelengths of the 69.93 , 69.98 and 70.05 \AA transitions were decoupled from the stronger 69.65 \AA feature. We found the best-fit location of the former group to be displaced by 0.04 \AA from the reference position, while the latter line lies very close to its expected location.

The relatively unexplored and complex nature of the crowded soft X-ray spectrum in the $50\text{--}75 \text{ \AA}$ wavelength range poses particular challenges for estimating line fluxes. In addition to the lines from the $n = 2$ shells of abundant elements such as Mg, Si, S and Ar, and the $n = 3$ shell of Fe, lines from shorter wavelengths arising from higher spectral orders are also present in this range. Unlike the *Chandra* ACIS CCD detector, the HRC-S microchannel plate detector possesses no energy resolution of its own and overlapping spectral orders cannot be separated. Prior to performing line fits we therefore looked for the presence of significant blends from known strong lines in higher orders.

The LETGS is designed with a grating bar-to-space ratio of 1:1, which results in some suppression of even orders. The most important order for line blends in the $50\text{--}75 \text{ \AA}$ range is the 3rd, which has an efficiency of about 10% that of 1st order.⁸ Two of the Fe XV lines in our list coincided reasonably closely with notable 3rd order lines: $\lambda 66.25$, which lies slightly less than one line width away from 3rd order O VII $\lambda 22.098$; and $\lambda 52.91$, which lies a line width away from 3rd order Fe XVIII $\lambda 17.62$. The O VII forbidden line is quite strong in the spectrum of Capella, and Fe XV $\lambda 66.25$ was therefore discarded. However Fe XVIII $\lambda 17.62$ is a much weaker line, of which there is no obvious sign in 3rd order. It arises between the levels $2s^2 2p^4 3p^2 P_{3/2}$ and $2s 2p^6^2 S_{1/2}$, and occurs because of configuration mixing (Drake et al. 1999).

Spectral orders 4 and 5 have similar efficiencies of 2–3 % that for 1st order. The O VIII + Fe XVIII $\lambda 16.00$ blend coincides in 4th order with Fe XV $\lambda 63.97$, and was included in the spectral fit with the relative wavelengths of the two components kept fixed. While there

⁸see <http://cxc.harvard.edu/cal/Letg/HO2004/>

are no other strong lines blended with our Fe XV features in 4th and 5th orders, there is a slew of weaker lines from $\Delta n > 0$ transitions in the $n = 2$ shells of Fe and Ni that fall in the 50–75 Å range. These transitions give rise to an additional pseudocontinuum, that we treated empirically through the estimation of a local continuum for each line or line group. Such empirical local continua were also guided by the broad-band “by eye” continuum, that can be seen in Figure 8.

In the fitting of some lines, neighbouring features blend in with the line wings. In most cases, these blending features are not clean lines that could be unambiguously identified with particular transitions of accurately known wavelengths, but are often complex blends with some unidentified contributions. To account for these unidentified transitions in the measured fluxes of our lines of interest, we added line components in an ad hoc fashion until the profiles of blended features could be empirically matched. Examples are shown in Figure 10, while the observed Fe XV line ratios are listed in Table 4, along with their associated errors. In Table 5 we list the wavelengths of the additional ad hoc line components.

As with the XSST observations (§ 3.1), the measured intensity of the 59.40 Å line is given in Table 4, and those of the other Fe XV transitions may be inferred from this using the line ratio values. It should be kept in mind in the interpretation of the measured fluxes that they are also prone to uncertainty caused by hidden blends of unidentified lines. For such cases, there is an expectation that the measured fluxes might be systematically too high.

4. Results and Discussion

In Tables 2 and 4 we list the observed Fe XV emission line ratios from the XSST solar flare spectrum and the *Chandra* Capella observations, respectively. Also shown in the tables are the theoretical results from Figures 1–7 at the temperature of maximum fractional abundance in ionization equilibrium for Fe XV, $T_e = 10^{6.3}$ K (Mazzotta et al. 1998), and at electron densities derived for the solar and Capella observations from emission line ratios in O VII (Brown et al. 1986; Phillips et al. 2001). The temperature-sensitive G -ratio for O VII in the XSST and Capella data indicates that $T_e = 10^{6.3}$ K in both features, similar to that of maximum fractional abundance for Fe XV. In the case of Capella, whose coronal emission measure distribution rises quite steeply to a peak at $T_e = 6 \times 10^6$ K (see, for example, Brickhouse et al. 2000), it is possible that this G -ratio slightly underestimates the mean temperature of line formation, as was found empirically by Testa, Drake & Peres (2004) for a sample of active stars. However, the ion populations of both O VII and Fe XV peak at very similar temperatures, and hence the O VII density should still accurately reflect that

of the Fe XV emitting region of the plasma. We have also verified that the slightly higher temperatures of line formation that would result from the relatively steep Capella emission measure distribution do not significantly change the predicted Fe XV line ratios from those listed in Table 4. The error bars on the theoretical results are based on the estimated $\pm 20\%$ accuracy of the line ratio calculations (see § 2).

An inspection of Table 2 reveals very good agreement between the XSST observations and the theoretical predictions for the ratios R_5 and R_7 . This indicates that the 63.97 and 69.65 Å lines are well detected in the XSST spectrum, and must be relatively free from blends. In particular, we confirm the identification by Bhatia et al. of the 63.97 Å feature as the $3p^2\ ^1D-3s4f\ ^1F$ transition of Fe XV, and not the Al VIII $2s^22p^2\ ^3P_{1,2}-2s2p^23p\ ^3D_{2,3}$ lines as originally classified by Acton et al. (1985). These authors also identify the 69.65 Å line as being partially due to Si VIII and Fe XIV transitions, with an unknown feature responsible for most of the line flux. However our result for R_7 clearly shows that the line is primarily the Fe XV $3s3p\ ^1P-3s4s\ ^1S$ transition, as suggested by Bhatia et al. We have confirmed this by generating a synthetic spectrum using CHIANTI, which indicates that the Si VIII $2s^22p^3\ ^4S-2s^22p^23s\ ^4P_{5/2}$ line only contributes about 15% to the total 69.65 Å flux, and that no Fe XIV transitions are present.

Similarly, the observed R_1 , R_9 , R_{10} , R_{11} and R_{12} ratios in Table 2 are only slightly larger than the theoretical values, indicating that the 52.91, 69.98, 70.05, 73.47 and 82.76 Å lines must be mostly due to Fe XV. Indeed, within the observational and theoretical errors in the line ratios, all the observed fluxes may arise from this ion. This is supported by the CHIANTI synthetic spectrum, which predicts no significant blending species for the 52.91, 69.98 and 70.05 Å features, and contributions of only about 10% from Ne VIII $1s^22p\ ^2P_{1/2}-1s^24d\ ^2D_{3/2}$ and 20% from Ne IX $1s2p\ ^1P-1s3s\ ^1S$ to the 73.47 and 82.76 Å lines, respectively. Our classification of the 82.76 Å feature as the Fe XV $3s3d\ ^3D_3-3s4p\ ^3P_2$ line is, to our knowledge, the first time this transition has been identified in an astrophysical source.

The good agreement between theory and observation for the above line ratios indicates that they should provide useful diagnostics for the Fe XV emitting region of a plasma. In particular, R_7 , R_9 , R_{10} and R_{11} are all temperature and/or density sensitive, and hence with careful use should allow these parameters to be derived. For example, R_7 could be employed to evaluate T_e , as it does not vary with N_e (Figure 1), and the latter could then be determined from R_{10} or R_{11} (Figures 6 and 7).

The observed values of R_2 , R_3 , R_4 , R_6 and R_8 in the XSST spectrum are all significantly larger than theory, implying that the 53.11, 55.78, 56.17, 66.25 and 69.93 Å lines of Fe XV are blended to varying degrees. For the 53.11 Å feature, the blending line contributes about

50% of the measured flux, and the CHIANTI synthetic spectrum indicates that this is most likely the S IX $2s^2 2p^4 \ ^3P_1-2p^3 3s \ ^3P_2$ transition. This is predicted to have an intensity of approximately 10% that of the Fe XVI $3p \ ^2P_{1/2}-4d \ ^2D_{3/2}$ line at 54.13 Å, i.e. about 16 photons $\text{cm}^{-2} \text{s}^{-1} \text{arcsec}^{-2}$. The measured flux of the 53.11 Å feature is 31 photons $\text{cm}^{-2} \text{s}^{-1} \text{arcsec}^{-2}$, so S IX should contribute 50%, in agreement with observation. We note that Acton et al. (1985) did not classify the 53.11 Å feature, the Fe XV identification being suggested by Bhatia et al. (1997). However we can now confirm that the line is the $3s^2 \ ^1S-3s4p \ ^3P_1$ transition of Fe XV, although it is blended.

For the 55.78 Å line, CHIANTI indicates that the Si X $2s2p^2 \ ^2S-2s2p3s \ ^2P_{1/2,3/2}$ and Si IX $2s^2 2p^2 \ ^3P_1-2s^2 2p3d \ ^1D$ transitions should together have an intensity about 70% that of the Fe XV line. Our observation of R₃ implies that the blending species may be stronger, and contribute about 150% of the Fe XV flux. However when the uncertainties in the experimental and theoretical R₃ ratios are taken into account, the data are compatible with a 70% contribution from Si X and Si IX. Similarly, a comparison of theory and observation for R₆ indicates that Fe XV only contributes about 10% to the intensity of the 66.25 Å feature. This is in agreement with CHIANTI, which predicts that 90% of the observed flux is due to the Fe XVI $3d \ ^2D_{3/2}-4f \ ^2F_{5/2}$ line.

By contrast, it is not clear from CHIANTI what the blending species are for the 56.17 and 69.93 Å lines, with no transitions predicted to have intensities more than 10% those of the relevant Fe XV features. It is however possible that the blending may be due to strong lines observed by XSST in second- or third-order, which are appearing in first-order at these wavelengths. For example, in the case of the 56.17 Å line, CHIANTI indicates no strong transitions in second-order (i.e. around 28.09 Å), but the intense Ca XVIII $1s^2 2s \ ^2S-1s^2 3p \ ^2P_{1/2}$ transition is predicted in third-order (18.73 Å). Similarly, for the 69.93 Å line there is a predicted third-order feature at 23.31 Å, namely the Ca XVI $2s2p^2 \ ^2P_{3/2}-2s2p3d \ ^2D_{5/2}$ transition. There are unfortunately no Ca XVIII lines in the XSST spectrum for comparison purposes, but there is a Ca XVI transition at 21.45 Å ($2s^2 2p \ ^2P_{1/2}-2s^2 3d \ ^2D_{3/2}$), with an intensity $I = 37 \text{ photons cm}^{-2} \text{s}^{-1} \text{arcsec}^{-2}$. However the predicted CHIANTI intensity ratio is $I(23.31 \text{ Å})/I(21.45 \text{ Å}) < 10^{-3}$, indicating that the Ca XVI 23.31 Å transition cannot be responsible for the blend in the 69.93 Å line. Clearly, the identification of the blends for the 56.17 and 69.93 Å features will require further work.

In the case of the *Chandra* observations of Capella, agreement between theory and experiment in Table 4 is very good for the majority of the line ratios. Where there are discrepancies, such as for R₈, these tend to mirror those found for the XSST spectrum, with the observed value being somewhat larger than theory, indicative of some blending. However, in most instances the observed line ratios actually show smaller discrepancies with

theory than do the XSST results. To a certain extent, such agreement may be judged to be unsurprising, as in our analysis of the Capella observations we added line components in an ad hoc fashion until the profiles of blending features could be empirically matched (see § 3.2). Nevertheless, our results indicate that profile fitting of the *Chandra* data, rather than simple measurements of emission line intensities, does allow the reliable detection of Fe XV soft X-ray features in the 50–75 Å wavelength range. Indeed, our work represents (to our knowledge) the first time that the Fe XV $n = 3$ –4 lines have been identified in an astrophysical source other than the Sun. Hopefully, our results will encourage the future use of these lines as plasma diagnostics for this spectral region.

In summary, we have performed a detailed analysis of Fe XV soft X-ray lines in the ~ 52 –83 Å wavelength region, observed in the solar spectrum by the XSST spectrograph, and confirmed identifications for several emission features and also detected a new transition. Additionally, the Fe XV lines have been measured in *Chandra* observations of Capella, and appear to provide potentially useful plasma diagnostics. We therefore hope that our work will stimulate renewed interest in this relatively unexplored spectral region, in particular through our provision of the co-added *Chandra* spectrum for Capella, which are probably the highest signal-to-noise data available. Many dozens of lines in the solar soft X-ray spectrum are without identifications, and the Capella spectrum (in combination with the XSST solar line list) should provide an aid to the identification of soft X-ray transitions and the investigation of their usefulness as plasma diagnostics. This will be important for future space missions, and in particular the EUV Variability Experiment (EVE), which is part of the *Solar Dynamics Observatory* (SDO), due for launch in 2008 ⁹. One of the EVE instruments is the Multiple EUV Grating Spectrograph (MEGS), which will observe the 50–1050 Å region at a spectral resolution of 1 Å. Clearly, the lines in this wavelength range will need to be identified and understood in advance of MEGS observations, as this instrument will not be able to resolve them individually.

K.M.A., R.S.I.R. and D.S.B. acknowledge financial support from the EPSRC and PPARC Research Councils of the United Kingdom. F.P.K. is grateful to AWE Aldermaston for the award of a William Penney Fellowship. The authors thank Peter van Hoof for the use of his Atomic Line List, and Jeffrey Linsky for very useful comments on an earlier version of the paper. CHIANTI is a collaborative project involving the Naval Research Laboratory (USA), Rutherford Appleton Laboratory (UK), and the Universities of Florence (Italy) and Cambridge (UK).

⁹See <http://lasp.colorado.edu/eve/>

REFERENCES

- Acton, L. W., Bruner, M. E., Brown, W. A., Fawcett, B. C., Schweizer, W., & Speer, R. J. 1985, *ApJ*, 291, 865
- Aggarwal, K. M., Keenan, F. P., & Msezane, A. Z. 2003, *A&A*, 410, 349
- Austin, W. E., Purcell, J. D., Tousey, R., & Widing, K. G. 1966, *ApJ*, 145, 373
- Bely, O., & Blaha, M. 1968, *Sol. Phys.*, 3, 563
- Bhatia, A. K., Mason, H. E., & Blancard, C. 1997, *At. Data Nucl. Data Tables*, 66, 83
- Behring, W. E., Cohen, L., & Feldman, U. 1972, *ApJ*, 175, 493
- Brickhouse, N. S., Dupree, A. K., Edgar, R. J., Liedahl, D. A., Drake, S. A., White, N. E., & Singh, K. P. 2000, *ApJ*, 530, 387
- Brown, W. A., Bruner, E. C., Acton, L. W., Franks, A., Stedman, M., & Speer, R. J. 1979, *Proc. SPIE*, 184, 278
- Brown, W. A., Bruner, M. E., Acton, L. W., & Mason, H. E. 1986, *ApJ*, 301, 981
- Bruner, E. C., Brown, W. A., Salat, S. W., Franks, A., Schmidtke, G., Schweizer, W., & Speer, R. J. 1980, *Opt. Eng.*, 19, 433
- Campbell, S. M., & Brickhouse, N. S. 2001, *Bulletin of the American Astronomical Society*, 33, 1329
- Chung, S. M., Drake, J. J., Kashyap, V. L., Ratzlaff, P. W., & Wargelin, B. J. 2004, *Proc. SPIE*, 5488, 51
- Churilov, S. S., Kononov, E. Y., Ryabtsev, A. N., & Zayikin, Y. F. 1985, *Phys. Scripta*, 32, 501
- Churilov, S. S., Levashov, V. E., & Wyart, J. F. 1989, *Phys. Scripta*, 40, 625
- Deb, N. C., Aggarwal, K. M., & Msezane, A. Z. 1999, *ApJS*, 121, 265
- Dere, K. P. 1978, *ApJ*, 221, 1062
- Dere, K. P., Landi, E., Mason, H. E., Monsignori-Fossi, B. C., & Young, P. R. 1997, *A&AS*, 125, 149
- Drake, J. J. 2004, *Chandra News*, 11, 8

- Drake, J. J., Swartz, D. A., Beiersdorfer, P., Brown, G. V., & Kahn, S. M. 1999, *ApJ*, 521, 839
- Dufton, P. L. 1977, *Comp. Phys. Commun.*, 13, 25
- Dufton, P. L., Berrington, K. A., Burke, P. G., & Kingston, A. E. 1978, *A&A*, 62, 111
- Dyall, K. G., Grant, I. P., Johnson, C. T., Parpia, F. A., & Plummer, E. 1989, *Comput. Phys. Commun.*, 55, 425
- Eissner, W., Jones, M., & Nussbaumer, H. 1972, *Comput. Phys. Commun.*, 8, 270
- Feldman, U., Mandelbaum, P., Seely, J. F., Doschek, G. A., & Gursky, H. 1992, *ApJS*, 81, 387
- Griffin, D. C., Badnell, N. R., Pindzola, M. S., & Shaw, J. A. 1999, *J. Phys. B*, 32, 2139
- Hibbert, A. 1975, *Comput. Phys. Commun.*, 9, 141
- Kashyap, V., & Drake, J. J. 2000, *Bulletin of the Astronomical Society of India*, 28, 475
- Kastner S.O., Bhatia A.K., 2001, *ApJ*, 553, 421
- Keenan, F. P., Mathioudakis, M., Pinfield, D. J., Brown, W. A., & Bruner, M. E. 1999, *Sol. Phys.*, 185, 289
- Laming, J. M., & Drake, J. J. 1999, *ApJ*, 516, 324
- Landman, D. A., & Brown, T. 1979, *ApJ*, 232, 636
- Litzen, U., & Redfors, A. 1987, *Phys. Scripta*, 36, 895
- Malinovsky, M., & Heroux, L. 1973, *ApJ*, 181, 1009
- Mazzotta, P., Mazzitelli, G., Colafrancesco, S., & Vittorio, N. 1998, *A&AS*, 133, 403
- Phillips, K. J. H., Mathioudakis, M., Huenemoerder, D. P., Williams, D. R., Phillips, M. E., & Keenan, F. P. 2001, *MNRAS*, 325, 1500
- Sugar, J., & Corliss, C. 1985, *J. Phys. Chem. Ref. Data Suppl.*, 2, 484
- Testa, P., Drake, J. J., & Peres, G. 2004, *ApJ*, 617, 508
- Thomas, R. J., & Neupert, W. M. 1994, *ApJS*, 91, 461

Weisskopf, M. C., Aldcroft, T. L., Bautz, M., Cameron, R. A., Dewey, D., Drake, J. J., Grant, C. E., Marshall, H. L., & Murray, S. S. 2003, *Experimental Astronomy*, 16, 1

Widing, K. G., & Sandlin, G. D. 1968, *ApJ*, 152, 545

Young, P. R., Del Zanna, G., Landi, E., Dere, K. P., Mason, H. E., & Landini, M. 2003, *ApJS*, 144, 135

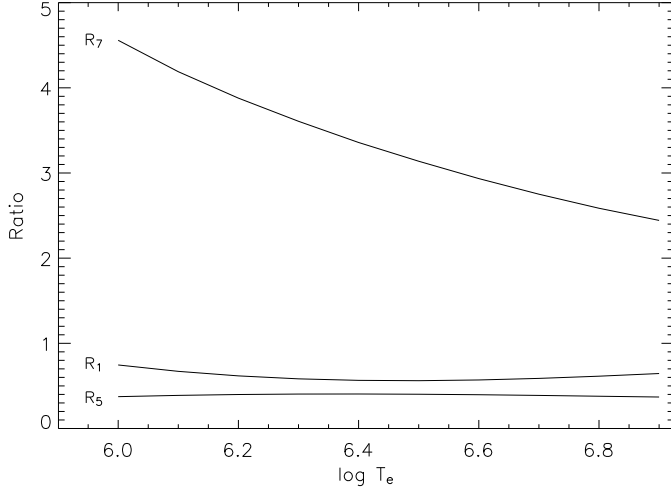


Fig. 1.— The theoretical Fe XV emission line intensity ratios $R_1 = I(52.91 \text{ \AA})/I(59.40 \text{ \AA})$, $R_5 = I(63.97 \text{ \AA})/I(59.40 \text{ \AA})$ and $R_7 = I(69.65 \text{ \AA})/I(59.40 \text{ \AA})$, where I is in photon units, plotted as a function of logarithmic electron temperature (T_e in K) at an electron density of $N_e = 10^{10} \text{ cm}^{-3}$. However we note that the line ratios are insensitive to the adopted electron density for $N_e = 10^8\text{--}10^{13} \text{ cm}^{-3}$.

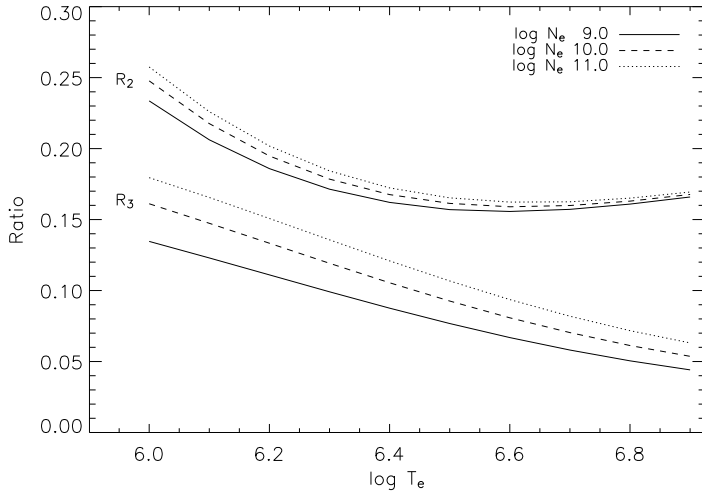


Fig. 2.— The theoretical Fe XV emission line intensity ratios $R_2 = I(53.11 \text{ \AA})/I(59.40 \text{ \AA})$ and $R_3 = I(55.78 \text{ \AA})/I(59.40 \text{ \AA})$, where I is in photon units, plotted as a function of logarithmic electron temperature (T_e in K) at logarithmic electron densities of $\log N_e = 9.0, 10.0$ and 11.0 (N_e in cm^{-3}).

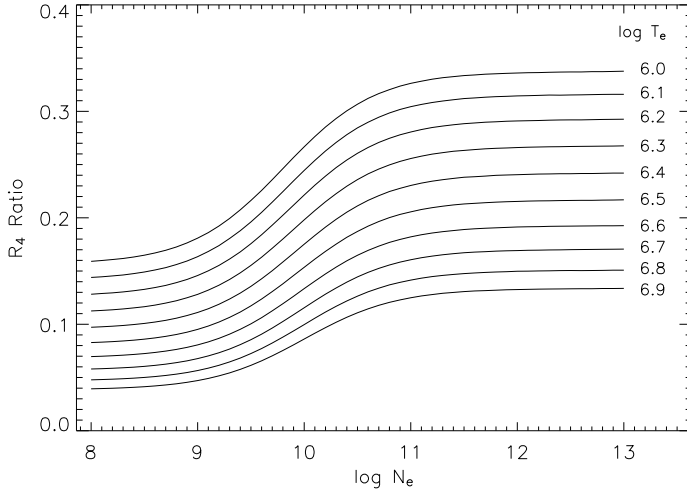


Fig. 3.— The theoretical Fe XV emission line intensity ratio $R_4 = I(56.17 \text{ \AA})/I(59.40 \text{ \AA})$, where I is in photon units, plotted as a function of logarithmic electron density (N_e in cm^{-3}) for several values of logarithmic electron temperature in the range $\log T_e = 6.0\text{--}6.9$ (T_e in K).

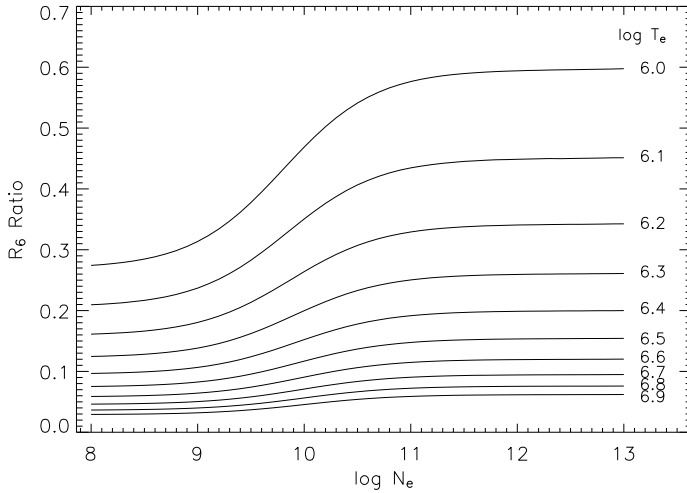


Fig. 4.— The theoretical Fe XV emission line intensity ratio $R_6 = I(66.25 \text{ \AA})/I(59.40 \text{ \AA})$, where I is in photon units, plotted as a function of logarithmic electron density (N_e in cm^{-3}) for several values of logarithmic electron temperature in the range $\log T_e = 6.0\text{--}6.9$ (T_e in K).

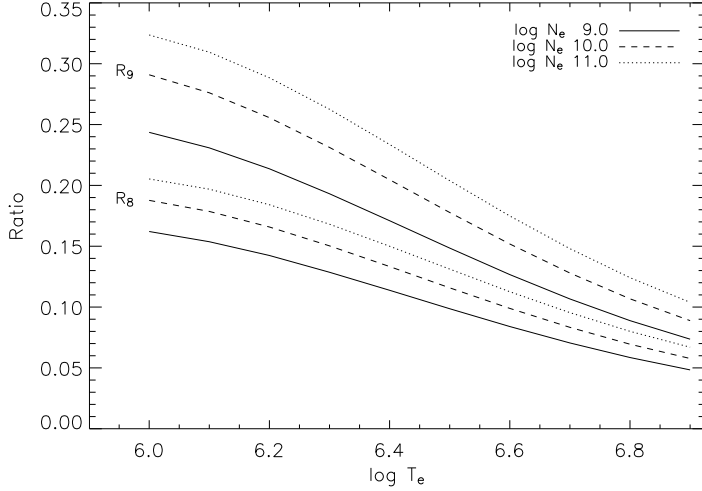


Fig. 5.— The theoretical Fe XV emission line intensity ratios $R_8 = I(69.93 \text{ \AA})/I(59.40 \text{ \AA})$ and $R_9 = I(69.98 \text{ \AA})/I(59.40 \text{ \AA})$, where I is in photon units, plotted as a function of logarithmic electron temperature (T_e in K) at logarithmic electron densities of $\log N_e = 9.0, 10.0$ and 11.0 (N_e in cm^{-3}).

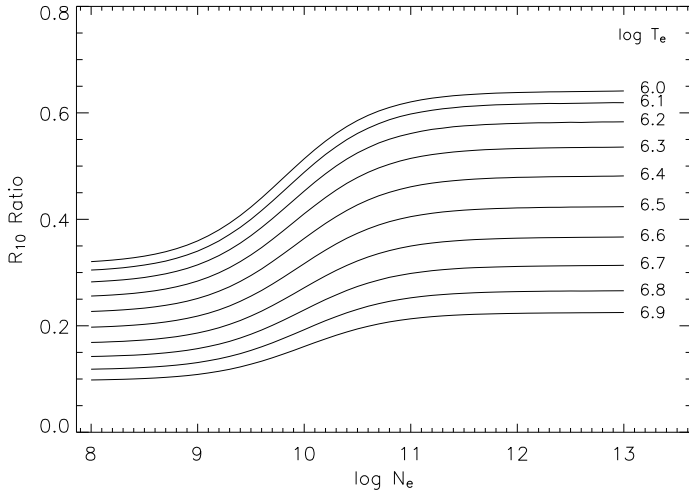


Fig. 6.— The theoretical Fe XV emission line intensity ratio $R_{10} = I(70.05 \text{ \AA})/I(59.40 \text{ \AA})$, where I is in photon units, plotted as a function of logarithmic electron density (N_e in cm^{-3}) for several values of logarithmic electron temperature in the range $\log T_e = 6.0\text{--}6.9$ (T_e in K).

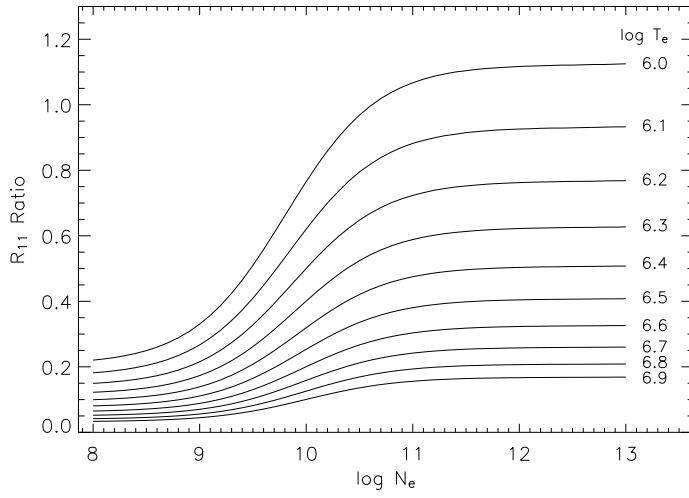


Fig. 7.— The theoretical Fe XV emission line intensity ratio $R_{11} = I(82.76 \text{ \AA})/I(59.40 \text{ \AA})$, where I is in photon units, plotted as a function of logarithmic electron density (N_e in cm^{-3}) for several values of logarithmic electron temperature in the range $\log T_e = 6.0\text{--}6.9$ (T_e in K).

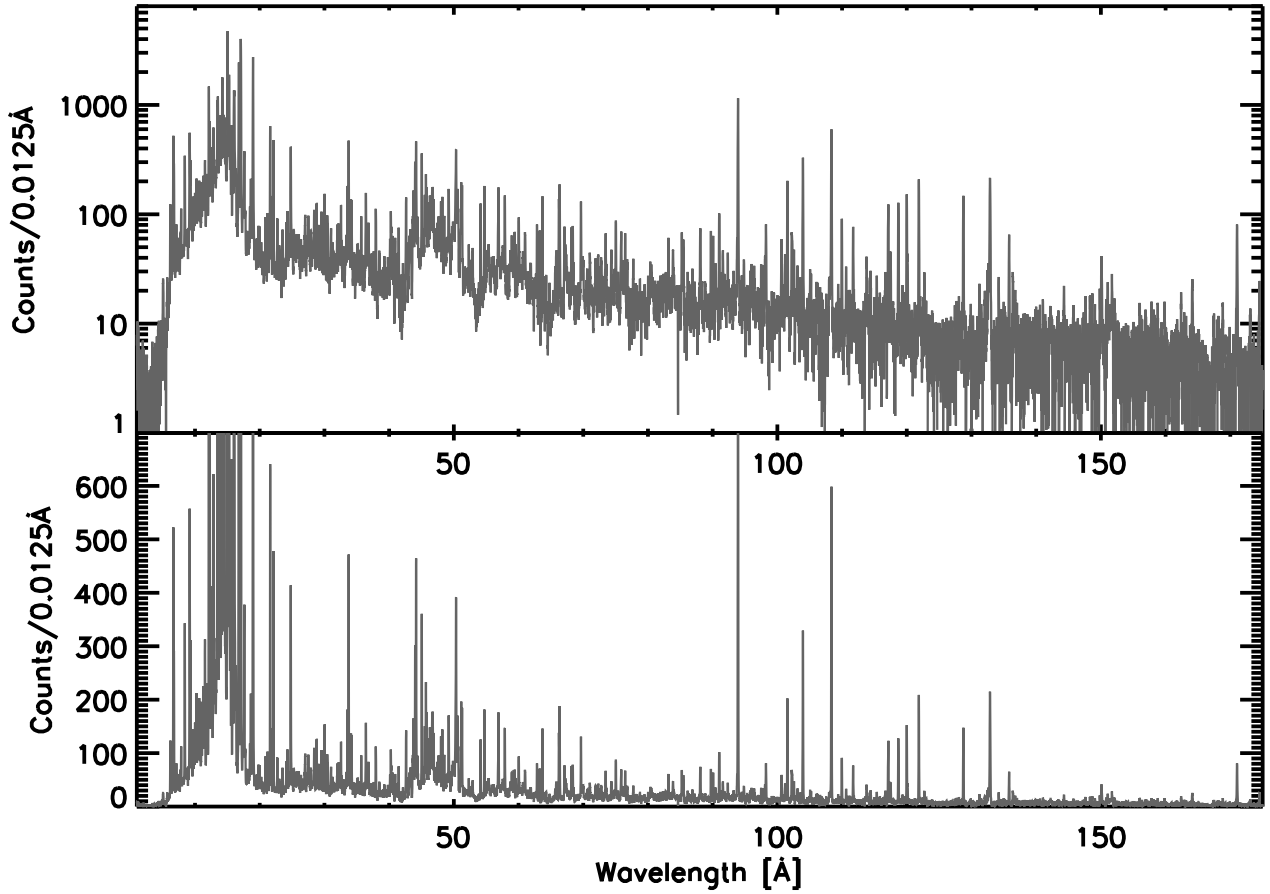


Fig. 8.— The co-added LETG+HRC-S spectrum of Capella in the 5–175 Å range. The top panel shows the full dynamic range of the spectrum, while the bottom panel is an expanded spectrum to more clearly show the emission features in the 25–175 Å soft X-ray wavelength region.

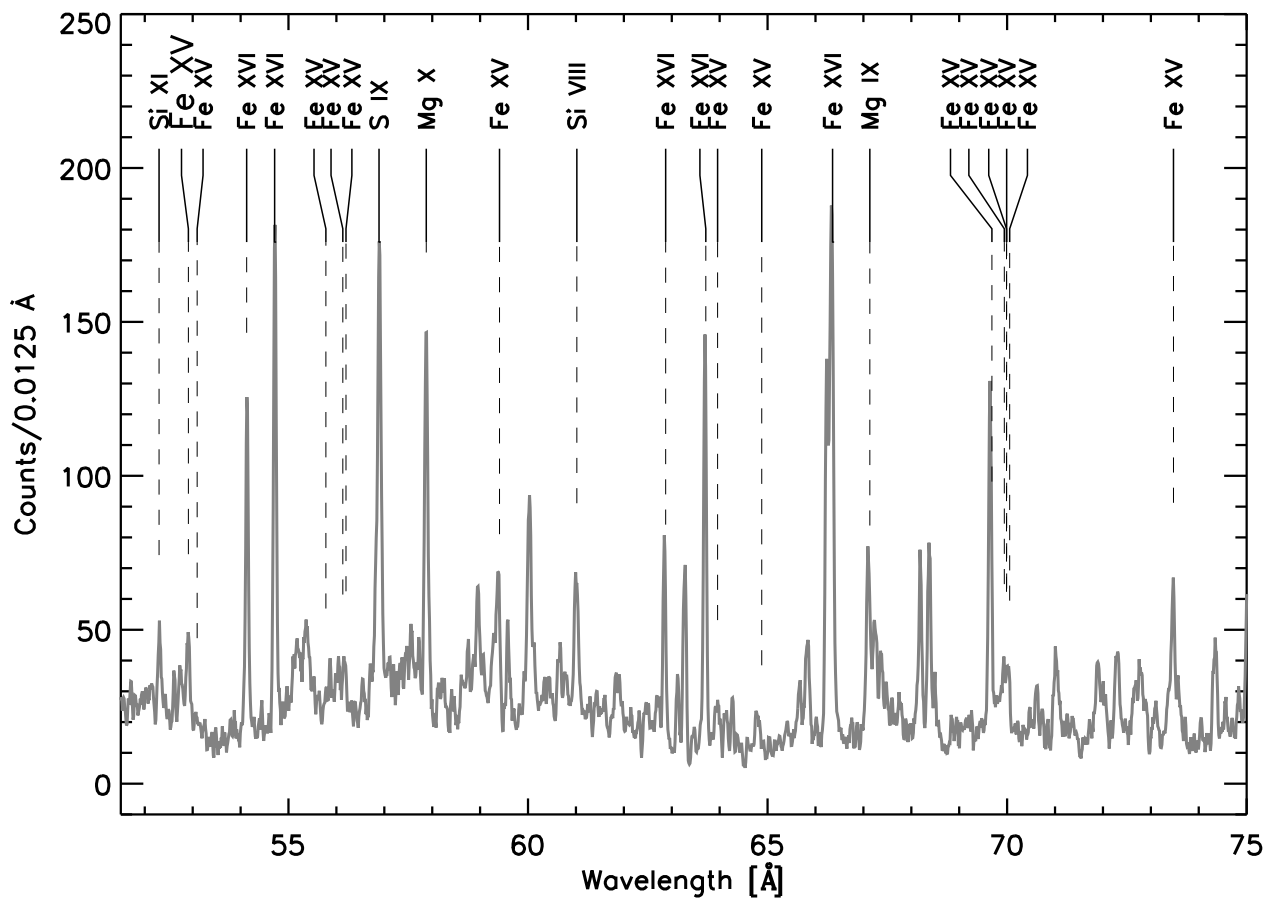


Fig. 9.— Portion of the co-added LETG+HRC-S spectrum of Capella in the 50–75 Å range. Lines of Fe XV analysed in the present paper are identified, together with some other prominent transitions of Fe, Mg, Si and S. The pseudo-continuum is comprised of a superposition of weak lines from the $n = 2$ levels of abundant elements, mostly Mg, Si, S and Ar, but also including contributions from the less abundant elements Na and Al.

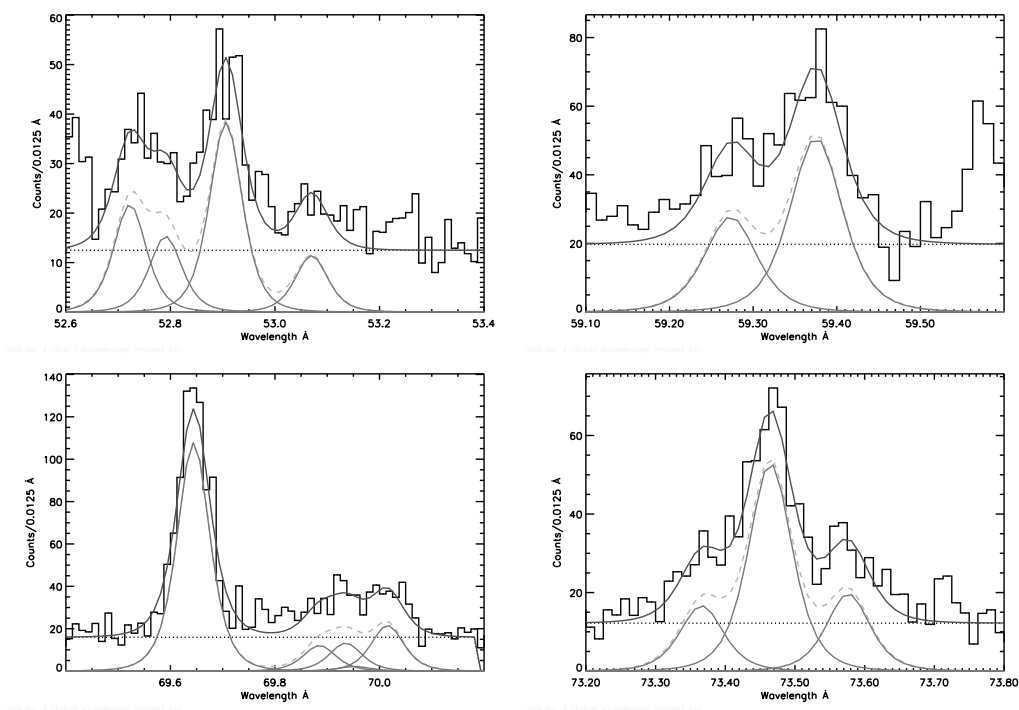


Fig. 10.— Example model fits to the 52.91, 53.11, 59.40, 69.65, 69.93, 69.98, 70.05 and 73.47 Å lines of Fe XV in the *Chandra* spectrum of Capella, from which the fluxes were estimated. Some lines required moderate deblending, which was achieved by the ad hoc addition of neighbouring lines in the model fit. Adopted pseudo-continua (dotted lines), together with individual line components and their sum, are also shown.

Table 1. Fe XV transitions in the XST solar flare spectrum and line ratio designations

Wavelength (Å)	Transition	R = I(λ)/I(59.40 Å)
52.91	$3s^2\ ^1S_0-3s4p\ ^1P_1$	R ₁
53.11	$3s^2\ ^1S_0-3s4p\ ^3P_1$	R ₂
55.78	$3s3p\ ^3P_1-3s4d\ ^3D_{1,2}$	R ₃
56.17	$3s3p\ ^3P_2-3s4d\ ^3D_3$	R ₄
59.40	$3s3p\ ^1P_1-3s4d\ ^1D_2$...
63.97	$3p^2\ ^1D_2-3s4f\ ^1F_3$	R ₅
66.25	$3s3p\ ^3P_2-3s4s\ ^3S_1$	R ₆
69.65	$3s3p\ ^1P_1-3s4s\ ^1S_0$	R ₇
69.93	$3s3d\ ^3D_1-3s4f\ ^3F_2$	R ₈
69.98	$3s3d\ ^3D_2-3s4f\ ^3F_{2,3}$	R ₉
70.05	$3s3d\ ^3D_3-3s4f\ ^3F_{3,4}$	R ₁₀
73.47	$3s3d\ ^1D_2-3s4f\ ^1F_3$	R ₁₂
82.76	$3s3d\ ^3D_3-3s4p\ ^3P_2$	R ₁₁

Table 2. Fe XV line ratios in the XSST solar flare spectrum

Line ratio	Observed ^a	Theoretical ^b
R ₁	0.78 ± 0.23	0.58 ± 0.12
R ₂	0.36 ± 0.11	0.18 ± 0.04
R ₃	0.33 ± 0.10	0.13 ± 0.03
R ₄	0.54 ± 0.16	0.23 ± 0.05
R ₅	0.35 ± 0.08	0.40 ± 0.08
R ₆	2.6 ± 0.8	0.23 ± 0.05
R ₇	3.0 ± 0.9	3.6 ± 0.7
R ₈	0.28 ± 0.08	0.16 ± 0.03
R ₉	0.33 ± 0.10	0.25 ± 0.05
R ₁₀	0.73 ± 0.22	0.46 ± 0.09
R ₁₁	0.75 ± 0.23	0.50 ± 0.10
R ₁₂	1.4 ± 0.4	1.2 ± 0.2

^aI(59.40 Å) = 85 photons cm⁻² s⁻¹ arcsec⁻².

^bDetermined from Figures 1–7 at T_e = 10^{6.3} K and N_e = 10^{10.4} cm⁻³.

Table 3. *Chandra* LETG+HRC-S observations of Capella employed in the present analysis

Obs (ID)	Exposure (ks)	Start Date (UT)	Start Time (UT)	End Date (UT)	End Time (UT)
58	34.11	2000-03-08	06:30:50	2000-03-08	16:25:31
62435	32.71	1999-09-06	00:27:21	1999-09-06	09:49:59
1009	26.97	2001-02-14	11:41:47	2001-02-14	19:27:44
1248	85.23	1999-11-09	13:28:25	1999-11-10	13:28:55
1420	30.19	1999-10-29	22:31:27	1999-10-30	07:29:02
3675	27.16	2003-09-28	04:23:10	2003-09-28	12:21:25

Table 4. Fe XV line ratios in the *Chandra* observations of Capella

Line ratio	Observed ^a	Theoretical ^b
R ₁	0.55 ± 0.06	0.58 ± 0.12
R ₂	0.16 ± 0.03	0.18 ± 0.04
R ₄	0.26 ± 0.06	0.21 ± 0.04
R ₅	0.39 ± 0.06	0.40 ± 0.08
R ₇	2.9 ± 0.2	3.6 ± 0.7
R ₈	0.28 ± 0.06	0.15 ± 0.03
R ₉	0.35 ± 0.07	0.24 ± 0.05
R ₁₀	0.49 ± 0.06	0.44 ± 0.09
R ₁₂	1.3 ± 0.1	1.2 ± 0.2

^aI(59.40 Å) = (9.7 ± 0.7) × 10⁻⁵ photons cm⁻² s⁻¹.

^bDetermined from Figures 1–7 at T_e = 10^{6.3} K and N_e = 10^{10.2} cm⁻³.

Table 5. Wavelengths of ad hoc line components used in the Capella analysis

Fe XV λ (Å)	Blend λ (Å)	Candidate identification
52.91	52.72	Fe XVII? Ni XVIII?
	52.79	Fe XVIII? S IX?
55.78	55.87	Si IX?
56.17	56.06	Ne IX? S IX? Fe XVII?
59.40	59.27	Fe XVII?
63.97	64.00	O VIII + Fe XVIII 4th order
73.47	73.37	
	73.58	Ne VIII?